Supporting Information for

Template Effects in Cu(I)-Bi(III) Iodide Double Perovskites: A Study of Crystal Structure, Film Orientation, Band Gap and Photocurrent Response

Le-Yu Bi,[1] Tian-Li Hu,[1] Mu-Qing Li,[1] Bo-Kai Ling,[1] Mohamed Saber Lassoued,[1] Yue-Qiao Hu,[2] Zhaoxin Wu,[3,4] Guijiang Zhou,[5] Yan-Zhen Zheng*,[1]

[1] Frontier Institute of Science and Technology (FIST), Xi'an Jiaotong University Shenzhen Research School, State Key Laboratory for Mechanical Behavior of Materials, MOE Key Laboratory for Nonequilibrium Synthesis of Condensed Matter, Xi'an Key Laboratory of Sustainable Energy and Materials Chemistry and School of Science, Xi'an Jiaotong University, Xi'an, Shaanxi 710054, P. R. China.

[2] Key Laboratory of Advanced Molecular Engineering Materials, Baoji University of Arts and Sciences, No. 1 Hi-Tec Avenue, Baoji 721013, P. R. China.

[3] Key Laboratory of Photonics Technology for Information, Key Laboratory for Physical Electronics and Devices of the Ministry of Education, Department of Electronic Science and Technology, School of Electronic and Information Engineering, Xi'an Jiaotong University, Xi'an, China

[4] Collaborative Innovation Center of Extreme Optics, Shanxi University, Taiyuan 030006, China

[5] Ministry of Education Key Laboratory for Nonequilibrium Synthesis and Modulation of Condensed Matter and Department of Chemistry, Faculty of Science, Xi'an Jiao Tong University, Xi'an 710049, P. R. China

Table of Contents

Table of Contents

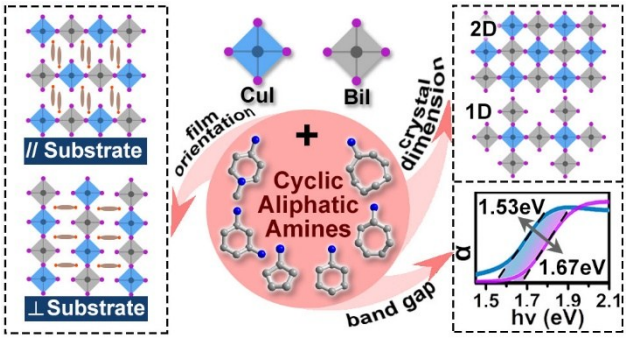

TOC description: Amine-dependent structural dimensions, energy band gaps and thin film orientations are revealed in seven newly pre-pared cuprous-bismuth iodide double perovskites.

Experimental Sections

Gerneral remarks

All reagents and solvents for the syntheses were purchased from commercial sources and used without further purification. PXRD intensities were measured at 293 K on a Rigaku D/max-IIIA diffractometer (Cu-K_α, λ =1.54056 Å). The crystalline powder samples were prepared by grinding the single-crystals and scanned from 2 theta = 5° to 60° at a rate of 10 °/min.

Syntheses of the compounds

(1,3-Diaminocyclohexane)$_2$BiCuI$_8$ 1 A slurry of Bi_2O_3 (0.5 mmol), CuI (1 mmol) Cyclohexane-1,4-diamine (14CDA) (2 mmol) and concentrated HI acid (5 ml) was heated at 130 °C for 20 hours in a PTFE reaction kettle, and then single crystals of **1** were grown by programmed cooling down to room temperature for 24 hours. The single crystals have a reddish black opaque color and a plate like shape (Figure S2). Crystals of **1** were washed with ethanol, and dried in vacuum (Yield: *ca*. 83 % based on Bi). Powder X-ray diffraction (PXRD) confirm the phase purity of the products (Figure S3).

(1-Methylpiperidin-4-amine)$_2$BiCuI$_8$ 2 Replacing 1,3-CDA in the synthesis of **1** with 1-methylpiperidin-4-amine (MPDA) produced euhedral crystals of **2** with opaque black color (Figure S2). The yield of **2** is about 86 % based on Bi. PXRD confirm the phase purity of the products (Figure S3).

(Cyclohexylamine)$_4$BiCuI$_8$ 3 Heating the mixture of Bi_2O_3 (0.5 mmol), CuI (1 mmol) Cyclohexylamine (CA) (4 mmol) and concentrated HI acid (5 ml) at 130 °C for 20 hours in a PTFE reaction kettle, and then single crystals of **3** was grown by programmed cooling down to room temperature for 24 hours. The single crystals have a black opaque color and a plate like shape (Figure S2). Crystals of **3** were suction filtered with petroleum ether, and dried in vacuum (Yield: *ca*. 88 % based on Bi). Powder X-ray diffraction (PXRD) confirm the phase purity of the products (Figure

S3).

(Cycloheptylamine)$_4$BiCuI$_8$ 4 Replacing the Cyclohexylamine (CA) in the synthesis of **3** with Cycloheptylamine (CHA) produced black long strip shape poly-crystals of **4**. The yields of **4** is *ca*. 52.4% based on Bi. PXRD confirm the phase purity of the products (Figure S3).

(Cyclooctylamine)$_4$BiCuI$_8$ 5 Replacing the Cyclohexylamine (CA) in the synthesis of **3** with Cyclooctylamine (COA) produced black long strip shape poly-crystals of **5**. The yields of **5** is *ca*. 81 % based on Bi. PXRD confirm the phase purity of the products (Figure S3).

(Cyclopentylamine)$_{10}$BiCu$_3$I$_{20}$ 6 Heated the mixture of Bi_2O_3 (0.5 mmol), CuI (1 mmol), cyclopentylamine (CPA) (4 mmol) and concentrated HI acid (5 ml) at 130 °C for 20 hours in a PTFE reaction kettle, and then single crystals of **6** was grown by programmed cooling down to room temperature for 24 hours. The single crystals have a reddish black opaque color and a strip like shape (Figure S2). Crystals of **6** were suction filtered with petroleum ether, and dried in vacuum (Yield: *ca*. 44 % based on Bi).

(Cyclopentylamine)$_7$BiCu$_2$I$_{14}$ 7 When adding excess CuI, compound **7** was obtained. The prescription of Bi_2O_3 (0.5 mmol), CuI (1.5 mmol), cyclopentylamine (CPA) (4 mmol) and concentrated HI acid (5 ml) was used (Yield: *ca*. 46 % based on Bi). The single crystals have a similar reddish black opaque color like that of **6**. Powder X-ray diffraction (PXRD) confirm the phase purity of all the products (Figure S3).

X-ray Crystallography

Single-crystal X-ray diffraction data collection for **1** - **7** were conducted on a Bruker SMART APEX II CCD diffractometer (Mo, λ = 0.71073 Å) by using the θ-ω scan technique at 150 K. The structures were solved by direct methods and refined with a full-matrix least-squares technique within the SHELXTL program package[1] and Olex2. The hydrogen atoms were set in calculated positions and refined using the

riding model. The crystallographic details are provided in Table S1, S2. Selected bond distances and bond angles are listed in Table S2. The crystallographic data for above compounds can be found in the Supporting Information or can be obtained free of charge from the Cambridge Crystallographic Data Centre via http://www.ccdc.cam.ac.uk/data_request/cif. CCDC Numbers: 1955022 (**1**), 1903596 (**2**), 1903595 (**3**), 1955914 (**4**), 1955920 (**5**), 1902928 (**6**), 1903048 (**7**). Due to the poor crystallization quality, the formation of two-dimensional polycrystalline sheets, and the disorder of cyclic organic molecules, we have not obtained perfect single crystal data for compound **4** and **5**, but inorganic frameworks can still be solved. And the PXRD data give farther proof for the SCXRD results.

Reference:

1. Sheldrick, G. *ActaCrystallogr. A* 2008, **64**, 112.

2. Dolomanov, O.V.; Bourhis, L.J.; Gildea, R.J.; Howard, J.A.K.; Puschmann, H.,*J. Appl. Cryst*., 2009, **42**, 339

Optical absorption measurement

Solid-state UV-Vis diffusion reflectance spectra for films and pressed powder samples were measured on a PE Lambda 950 UV-Vis-NIR spectrophotometer using $BaSO_4$ powder as the reflectance reference. The absorption spectra were calculated from reflectance spectra by the Kubelka-Munk function: $F(R) = \alpha/S = (1-R)^2/2R$, where R, α, and S are the coefficients for the reflection, the absorption and the scattering, respectively. Room-temperature steady-state emission spectra (PL) were collected on crystal samples using an Edinburgh FLS9 fluorimeter upon 630 nm excitation. 650 nm filter was used to reduce the noise.

The absorption onsets of films blue shifted from those of powder samples for the same compound. The exact reason for this blue shift is still unclear. We thought this related to the size of the compound. Instead of quantum confinement effect, we found scattering and absorption of incident light are causes of size dependent color change

of this series of CuBiI DPs. The relationship between color and particle size is well studied according to Mie scattering in many fields, and the pigment is one of the fields that related to this topic. As Dimitrije Radjenović et al. reported, after grinding, several colored materials (like copper(II) sulfate pentahydrate, cobalt(II) chloride hexahydrate, brown rosin and yellow rosin) get more light colors close to white.[1] Such phenomena are studied by many groups, they all owe the size dependent color change to the Mie scattering.[2-4] Not only in the mineral pigments but also in the hybrid perovskite was this phenomena discovered. Karunadasa et al. reported the absorption spectra of $(BA)_4AgBiBr_8$, $(BA)_2CsAgBiBr_8$, $Cs_2AgBiBr_6$ films all blue shifted for 0.3 to 0.5 eV than powder samples.[5] No matter for the film or the loose powder, complex surface morphology will introduce much scattering on crystal boundaries. So only after excluding the scattering can we obtain the intrinsic optical properties. One way is to test the UV-vis spectrum on single crystal, and another is to test on the pressed pellet which excludes the air among the particles and has a smooth surface. So we considered the absorption onsets of pressed powder rather than that of films as the band gaps.

Computational methods. All density-functional theory (DFT) calculations were carried out within the Materials Studio. The crystallographic data of compounds **1 - 7** obtained from Single Crystal XRD tests was used to calculate the electronic band structures and the densities of the states (DOSs). The ab initio calculations of the band structure, DOS and partial DOS (PDOS) were performed using the CASTEP. Before the calculation, geometric optimization was carried out until the energy fluctuation below 2×10^{-5} eV/atom and residual forces on the nuclei were below 0.05 eV/Å in magnitude. The exchange-correlation energy was calculated using Perdew-Burke-Ernzerhof (PBE) modification to the generalized gradient approximation (GGA).[6] The convergence threshold for the self-consistent field was 2×10^{-6} eV/atom. The pseudopotential form was OTFG ultrasoft mode and the energy cutoff was 489.8 eV. The Brillouin zone has been sampled with a highly-converged (0.015 /Å) set of k

points, using grids up to (2 × 2 × 2) points according to the Monkhorst Pack scheme[7] for all calculations.

Film Fabrication. Crystals (0.5 g) of each compound obtained by sol-vothermal reactions were dissolved in anhydrous DMF (1 ml), and black solutions without Dindal effect were obtained. ITO glass or ordinary glass was washed with detergent, and then ultrasonically bathed in deionized water, acetone and isopropyl alcohol for 15 minutes each. And ultraviolet ozone cleaning was performed for the slides for 30 minutes. The solutions were spin coated at 2000 rpm for 60 seconds with an acceleration of 1000 rpm/s. After annealing at 70 °C on a hot plate for 10 minutes, obvious color change from light yellow to dark red can be observed. Powder X-ray diffrac-tion (PXRD) confirm the phase purity of the products (Figure 3).

Electrical measurements. Pellets of pressed powder of **3** were used for the electron conductivity measurements under different temperatures and photo response measurements. 200 mg powder was used to press each pellet (ϕ = 12 mm) with the thickness about 0.3 mm. We used silver conductive paint (SPI supplies co.) to make current collectors and to attach the silver-clad copper wires to the pellets. Because the samples' resistances in this system were as high as 10^6 Ω, contact resistances between pellet sample, silver paint and wires were negligible. For that reason, two-probe measurements were adopted. We used a source meter (Keithley 2400) serving as a voltage source, and in series with a picoammeter (Keithley 6485) to detect the small currents.

To test the conductivity under different temperatures, we used an oven to control the temperature. Connect the positive and negative poles to the upper and lower surfaces of the pellets, like the Scheme 1a.

To test the photo-response, the positive and negative poles were attached to the same side of pellets. The areas of silver paint weere two semicircles, and one narrow strip like area was left without paint which could receive light from the lamp, see the Scheme 1b. A 350 W solar-simulating Xenon lamp was used as light source and we

used a bias voltage of 3 V. For every 40 s we blocked or unblocked the light and detected the current change.

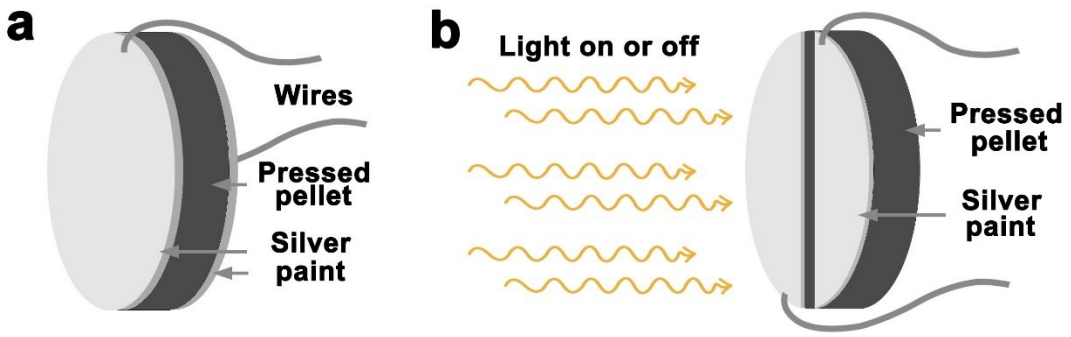

Scheme 1. (a) Conductivity test device under different temperature. (b) Photo-response test device.

Reference:

1. D. Radjenović, B. S. , B. R. , and and M. Radmilović-Radjenović, *American Journal of Engineering Research (AJER)*, 2018, **7**, 97.
2. A. P. Prishivalko, *Journal of Applied Spectroscopy*, 1996, **63**, 675-683.
3. M. Elias, *Appl. Opt.*, 2011, **50**, 2464-2473.
4. A. M. Gueli, G. Bonfiglio, S. Pasquale and S. O. Troja, *Color Research & Application*, 2017, **42**, 236-243.
5. B. A. Connor, L. Leppert, M. D. Smith, J. B. Neaton and H. I. Karunadasa, *J. Am. Chem. Soc.*, 2018, **140**, 5235-5240.
6. J. P. Perdew, K. Burke and M. Ernzerhof, *Physical Review Letter*, 1996, **77**, 3865--3868.
7. H. J. Monkhorst and J. D. Pack, *Physical Review B*, 1976, **13**, 5188-5192.

Table S1 Summary of crystal data and structural refinements for **1 - 4**

	1	2	3	4
Empirical formula	$C_{12}H_{34}BiCuI_8N_4O$	$C_{12}H_{32}BiCuI_8N_4$	$C_{24}H_{58}BiCuI_8N_4O$	$C_{27}H_{62}BiCuI_8N_4$
Formula weight	1538.15	1520.13	1706.46	1680.53
Crystal system	monoclinic	monoclinic	monoclinic	triclinic
Space group	C2/c	P2/n	I2/a	P-1
a/Å	22.259(13)	8.474(4)	19.688(3)	12.856(6)
b/Å	8.575(5)	10.137(5)	8.6011(16)	13.245(6)
c/Å	19.643(12)	18.767(9)	26.531(3)	14.790(6)
α/°	90	90	90	101.863(6)
β/°	119.160(6)	100.642(7)	92.146(15)	102.110(5)
γ/°	90	90	90	96.463(5)
Volume/Å^3	3274(3)	1584.4(13)	4489.6(12)	2377.8(18)
Z	4	2	4	2
ρ_{calc}g/cm^3	3.120	3.186	2.525	2.417
μ/mm^{-1}	13.572	14.019	9.911	9.357
F(000)	2712.0	1336	3096	1576.0
Reflections	18155	12413	20928	24609
Independent reflections	3739 [R_{int} = 0.0498, R_{sigma} =	2780 [Rint = 0.0321, Rsigma =	3947 [Rint = 0.0490, Rsigma =	8252 [R_{int} = 0.0469, R_{sigma} =
Data/restraints/parameters	3739/0/130	2780/0/126	3947/2/188	8252/64/223
Goodness-of-fit on F^2	1.013	1.071	1.102	1.042
Final R indexes [I>=2σ (I)]	R_1 = 0.0410, wR_2 = 0.0963	R_1 = 0.0282, wR_2 = 0.0658	R_1 = 0.0357, wR_2 = 0.0987	R_1 = 0.0953, wR_2 = 0.2576
Final R indexes [all data]	R_1 = 0.0613, wR_2 = 0.1058	R_1 = 0.0316, wR_2 = 0.0673	R_1 = 0.0454, wR_2 = 0.1050	R_1 = 0.1226, wR_2 = 0.2800

Table S2 Summary of crystal data and structural refinements for **5 - 7**

	5	6	7
Empirical formula	$C_{32}H_{72}BiCuI_8N_4$	$C_{50}H_{120}Bi_3CuI_{20}N_1$	$C_{35}H_{84}Bi_2CuI_{14}N_7$
Formula weight	1800.65	4090.03	2861.5
Crystal system	triclinic	triclinic	triclinic
Space group	P-1	P-1	P-1
a/Å	13.101(5)	13.158(9)	13.095(3)
b/Å	13.284(5)	13.635(9)	13.104(3)
c/Å	31.535(12)	16.187(11)	21.020(4)
α/°	98.500(5)	77.886(9)	90.340(3)
β/°	98.541(5)	67.137(9)	91.751(3)
γ/°	96.146(5)	75.691(9)	102.207(3)
Volume/Å^3	5321(4)	2572(3)	3523.6(12)
Z	2	1	1
ρ_{calc}g/cm^3	2.248	2.641	2.617
μ/mm^{-1}	8.368	11.354	11.440
F(000)	1656.0	1828.0	2393.0
Reflections	23283	23252	44338

Independent reflections	9986 [R_{int} = 0.0502, R_{sigma} =	8799 [R_{int} = 0.0659, R_{sigma} =	16244 [Rint = 0.0386, Rsigma =
Data/restraints/parameters	9986/83/239	8799/18/267	16244/1/661
Goodness-of-fit on F^2	1.038	1.009	1.001
Final R indexes [I>=2σ (I)]	R_1 = 0.0993, wR_2 = 0.2813	R_1 = 0.0568, wR_2 = 0.1368	R_1 = 0.0423, wR_2 = 0.0940
Final R indexes [all data]	R_1 = 0.1596, wR_2 = 0.3173	R_1 = 0.1239, wR_2 = 0.1740	R_1 = 0.0638, wR_2 = 0.1037

Table S3 Selected bond lengths (Å) and angles (°) for **1 - 3**

1		**2**		**3**	
Bi1-I2	3.0592(19)	Bi1-I3^1	3.0890(15)	Bi1-I3	3.0806(6)
Bi1-I2^1	3.0592(19)	Bi1-I3	3.0889(15)	Bi1-I3^1	3.0806(6)
Bi1-I3	3.060(2)	Bi1-I2	3.0859(12)	Bi1-I2^1	3.0677(7)
Bi1-I3^1	3.060(2)	Bi1-I2^1	3.0859(12)	Bi1-I2	3.0677(7)
Bi1-I4	3.090(3)	Bi1-I4	3.0778(12)	Bi1-I1	3.1111(7)
Bi1-I4^1	3.090(3)	Bi1-I4^1	3.0778(12)	Bi1-I1^1	3.1112(7)
I2-Cu1	3.041(6)	I2-Cu1	2.928(3)	I3-Cu1	2.750(3)
I1-Cu1^2	2.482(3)	I1-Cu1	2.5301(17)	I3^1-Bi1-I3	180
I2^1-Bi1-I2	180.0	I1-Cu2^2	2.4695(16)	I3-Bi1-I1^1	87.501(19)
I3-Bi1-I2^1	88.17(5)	I4-Cu2	2.935(3)	I3^1-Bi1-I1	87.502(19)
I3^1-Bi1-I2	88.17(5)	Cu1-I2^3	2.928(3)	I3^1-Bi1-I1^1	92.497(19)
I3-Bi1-I2	91.83(5)	Cu1-I13	2.5302(17)	I3-Bi1-I1	92.50(2)
I3^1-Bi1-I2^1	91.83(5)	Cu1-Cu2^2	1.676(5)	I2^1-Bi1-I3	88.023(19)
I3^1-Bi1-I3	180.0	Cu2-I1^4	2.4695(16)	I2-Bi1-I3	91.977(19)
I4^1-Bi1-I2	87.60(6)	Cu2-I1^5	2.4695(16)	I2^1-Bi1-I3^1	91.978(19)
I4^1-Bi1-I2^1	92.40(6)	Cu2-I4^6	2.935(3)	I2-Bi1-I3^1	88.023(19)
I4-Bi1-I2	92.40(6)	Cu2-Cu1^4	1.676(5)	I2^1-Bi1-I2	180
I4-Bi1-I2^1	87.60(6)	I3-Bi1-I3^1	177.72(2)	I2-Bi1-I1	89.826(18)
I4-Bi1-I3	89.81(5)	I21-Bi1-I3	91.001(14)	I^{2}1-Bi1-I1	90.172(18)
I4^1-Bi1-I3^1	89.81(5)	I2-Bi1-I3	87.433(14)	I2-Bi1-I11	90.175(18)
I4-Bi1-I3^1	90.19(5)	I21-Bi1-I3^1	87.433(14)	I2^1-Bi1-I1^1	89.827(18)
I4^1-Bi1-I3	90.19(5)	I2-Bi1-I3^1	91.001(14)	I1-Bi1-I1^1	180
I4^1-Bi1-I4	180.0	I21-Bi1-I2	93.51(4)	Cu1-I3-Bi1	159.57(7)
Cu1-I2-Bi1	164.29(7)	I4-Bi1-I3	91.227(15)	Cu1-I4-Cu1^2	31.54(17)
I2^2-Cu1-I2	103.4(3)	I4-Bi1-I3^1	90.430(14)	I4^2-Cu1-I3	110.51(11)
I1^2-Cu1-I2^2	101.12(13)	I4^1-Bi1-I3^1	91.226(15)	I4-Cu1-I3	104.35(11)
I1-Cu1-I2^2	93.13(12)	I4^1-Bi1-I3	90.431(14)	I4-Cu1-I4^2	143.25(14)
I1^2-Cu1-I2	93.13(12)	I4^1-Bi1-I2^1	176.491(1	Cu1^2-Cu1-I3	131.45(9)
I1-Cu1-I2	101.12(13)	I4-Bi1-I2^1	89.76(4)	Cu1^2-Cu1-I4	78.6(3)
I1-Cu1-I1^2	157.0(4)	I4^1-Bi1-I2	89.76(4)	Cu1^2-Cu1-I4^2	69.9(3)
		I4-Bi1-I2	176.491(1		
		I4-Bi1-I4^1	87.01(4)		
		Cu1-I2-Bi1	170.38(2)		
		Cu2^2-I1-Cu1	39.15(11)		
		Cu2-I4-Bi1	168.22(3)		
		I2-Cu1-I2^3	86.99(10)		
		I1-Cu1-I2^3	108.95(4)		
		I1-Cu1-I2	101.99(4)		
		I1^3-Cu1-I2	108.95(4)		
		I1^3-Cu1-I2^3	101.99(4)		
		I1-Cu1-I1^3	136.94(14)		
		Cu2^2-Cu1-I2	136.50(5)		
		Cu2^2-Cu1-I2^3	136.50(5)		
		Cu2^2-Cu1-I1^3	68.47(7)		

	$Cu2^{2}$-Cu1-I1	68.47(7)	
	$I1^{4}$-Cu2-$I1^{5}$	144.75(16)	
	$I1^{5}$-Cu2-$I4^{6}$	106.36(5)	
	$I1^{5}$-Cu2-I4	97.40(4)	
	$I1^{4}$-Cu2-$I4^{6}$	97.40(4)	
	$I1^{4}$-Cu2-I4	106.36(5)	
	I4-Cu2-$I4^{6}$	94.65(11)	
	$Cu1^{4}$-Cu2-$I1^{4}$	72.38(8)	
	$Cu1^{4}$-Cu2-$I1^{5}$	72.38(8)	
	$Cu1^{4}$-Cu2-I4	132.67(6)	
	$Cu1^{4}$-Cu2-$I4^{6}$	132.67(6)	
^{1}-X,1-Y,-Z; 21/2-X,+Y,-Z	^{1}3/2-X,+Y,1/2-Z; ^{2}-1+X,1+Y,+Z; ^{3}1/2-X,+Y,1/2-Z; ^{4}1+X,1+Y,+Z; ^{5}3/2-X,-1+Y,1/2-Z; ^{6}5/2X,+Y,1/2-Z		^{1}-X,1-Y,-Z; ^{2}1/2-X,+Y,-Z

Table S4 Selected bond lengths (Å) and angles (°) for **4** - **7**

4		**5**		**6**		**7**	
Bi1-I7	3.095(2)	Bi1-I1	3.111(6)	$Bi1-I1^{1}$	3.093(3)	Bi1-I1	2.9850(9)
Bi1-I6	3.015(2)	Bi1-I2	3.079(5)	Bi1-I1	3.093(3)	Bi1-I2	3.0932(9)
Bi1-I5	3.097(2)	Bi1-I3	3.029(5)	Bi1-I2	3.097(3)	Bi1-I3	3.0741(9)
Bi1-I4	3.075(2)	Bi1-I4	3.092(6)	$Bi1-I2^{1}$	3.097(3)	Bi1-I4	3.0869(9)
Bi1-I8	3.078(2)	Bi1-I5	3.085(5)	$Bi1-I3^{1}$	3.103(4)	Bi1-I5	3.0620(9)
$Bi1-I2^{1}$	3.131(2)	Bi1-I6	3.141(6)	Bi1-I3	3.103(4)	Bi1-I6	3.1701(9)
I4-Cu1	3.223(8)	Bi2-I9	3.085(5)	Bi2-I4	3.004(4)	Bi2-I9	3.0058(8)
I1-Cu1	2.457(5)	Bi2-I10	3.144(5)	Bi2-I5	3.033(4)	Bi2-I10	3.1774(9)
I2-Bi11	3.131(2)	Bi2-I11	3.164(6)	Bi2-I6	3.163(4)	Bi2-I11	2.9651(8)
I2-Cu1	2.845(6)	Bi2-I12	3.010(6)	Bi2-I7	3.205(4)	Bi2-I12	3.0257(8)
I3-Cu1	2.496(5)	Bi2-I13	3.040(6)	Bi2-I8	2.958(3)	Bi2-I13	3.2953(9)
I7-Bi1-I5	179.22(5)	Bi2-I14	3.086(5)	Bi2-I9	3.319(3)	Bi2-I14	3.1688(8)
$I7-Bi1-I2^{1}$	89.27(5)	$I2-Cu3^{1}$	2.96(3)	I10-Cu1	2.486(3)	$I3-Cu1^{1}$	3.282(3)
I6-Bi1-I7	91.66(5)	$I5-Cu2^{2}$	3.40(5)	$Cu1-I10^{2}$	2.486(3)	I6-Cu1	2.8332(18)
I6-Bi1-I5	88.95(5)	I6-Cu1	2.946(17)	$I1^{1}$-Bi1-I1	180.0	I7-Cu1	2.4943(16)
I6-Bi1-I4	88.53(5)	I7-Cu1	2.476(17)	I1-Bi1-I21	90.29(8)	I8-Cu1	2.4961(17)
I6-Bi1-I8	92.92(5)	I8-Cu1	2.425(16)	$I1^{1}$-Bi1-I21	89.71(8)	I9-Cu1	3.463(3)
$I6-Bi1-I2^{1}$	177.05(6)	$I10-Cu2^{2}$	2.70(3)	I1-Bi1-I2	89.72(8)	$Cu1-I1^{2}$	4.279(2)
$I5-Bi1-I2^{1}$	90.14(5)	$I10-Cu3^{2}$	2.98(2)	I11-Bi1-I2	90.28(8)	I1-Bi1-I2	90.925(19)
I4-Bi1-I7	89.24(5)	$Cu1-I3^{3}$	4.165(17)	I1-Bi1-I31	91.91(9)	I1-Bi1-I3	93.10(3)
I4-Bi1-I5	91.25(5)	$Cu1-I14^{4}$	3.325(17)	$I1^{1}$-Bi1-I31	88.09(9)	I1-Bi1-I4	92.09(2)
I4-Bi1-I8	178.24(6)	I15-Cu2	2.58(3)	$I1^{1}$-Bi1-I3	91.91(9)	I1-Bi1-I5	91.75(2)
$I4-Bi1-I2^{1}$	88.68(6)	I15-Cu3	2.472(17)	I1-Bi1-I3	88.09(9)	I1-Bi1-I6	178.46(2)
I8-Bi1-I7	89.72(5)	I16-Cu2	2.47(3)	I2-Bi1-I21	180.0	I2-Bi1-I6	87.822(19)
I8-Bi1-I5	89.77(5)	I16-Cu3	2.484(18)	I2-Bi1-I3	91.11(9)	I3-Bi1-I2	88.66(3)
$I8-Bi1-I2^{1}$	89.89(6)	$Cu2-I2^{5}$	3.84(5)	$I2-Bi1-I3^{1}$	88.89(9)	I3-Bi1-I4	88.30(3)
Bi1-I4-Cu1	170.01(12)	$Cu2-I10^{3}$	2.70(3)	$I2^{1}$-Bi1-$I3^{1}$	91.11(9)	I3-Bi1-I6	85.98(2)
$Cu1-I2-Bi1^{1}$	159.54(12)	$Cu3-I2^{5}$	2.96(3)	$I2^{1}$-Bi1-I3	88.89(9)	I4-Bi1-I2	175.83(2)
I1-Cu1-I4	94.4(2)	$Cu3-I10^{3}$	2.98(2)	$I3^{1}$-Bi1-I3	180.0	I4-Bi1-I6	89.11(2)
I1-Cu1-I2	102.1(2)	I1-Bi1-I6	89.85(16)	I4-Bi2-I5	88.40(10)	I5-Bi1-I2	94.16(2)
I1-Cu1-I3	150.5(2)	I2-Bi1-I1	89.85(17)	I4-Bi2-I6	171.44(11)	I5-Bi1-I3	174.35(2)
I2-Cu1-I4	99.20(18)	I2-Bi1-I4	91.62(18)	I4-Bi2-I7	84.69(10)	I5-Bi1-I4	88.63(2)
I3-Cu1-I4	93.9(2)	I2-Bi1-I5	177.33(17)	I4-Bi2-I9	85.69(9)	I5-Bi1-I6	89.24(2)
I3-Cu1-I2	104.46(18)	I2-Bi1-I6	88.64(17)	I5-Bi2-I6	98.95(10)	I9-Bi2-I10	85.776(17)
		I3-Bi1-I1	90.31(17)	I5-Bi2-I7	172.12(11)	I9-Bi2-I12	89.708(18)
		I3-Bi1-I2	89.72(16)	I5-Bi2-I9	86.43(9)	I9-Bi2-I13	86.95(2)
		I3-Bi1-I4	88.52(17)	I6-Bi2-I7	87.68(9)	I9-Bi2-I14	171.769(19)

	I3-Bi1-I5 92.66(15) I3-Bi1-I6 178.35(18) I4-Bi1-I1 178.12(18) I4-Bi1-I6 91.35(17) I5-Bi1-I1 88.94(15) I5-Bi1-I4 89.64(16) I5-Bi1-I6 88.98(16) I9-Bi2-I10 89.52(14) I9-Bi2-I11 89.90(16) I9-Bi2-I14 177.94(16) I10-Bi2-I11 87.46(15) I12-Bi2-I9 92.81(17) I12-Bi2-I10 176.40(19) I12-Bi2-I11 89.80(17) I12-Bi2-I13 90.37(19) I12-Bi2-I14 89.14(18) I13-Bi2-I9 90.46(16) I13-Bi2-I10 92.35(18) I13-Bi2-I11 179.59(18) I13-Bi2-I14 90.18(16) I14-Bi2-I10 88.50(16) I14-Bi2-I11 89.45(16) Cu3[1]-I2-Bi1 167.1(4) Bi1-I5-Cu2[2] 168.6(6) Cu1-I6-Bi1 160.4(4) Cu2[2]-I10-Bi2 156.6(9) Cu3[2]-I10-Bi2 164.4(4) I6-Cu1-I33 168.8(6) I6-Cu1-I14[4] 96.4(5) I7-Cu1-I33 78.4(4) I7-Cu1-I6 100.7(5) I7-Cu1-I14[4] 93.1(5) I8-Cu1-I3[3] 77.2(4) I8-Cu1-I6 106.2(6) I8-Cu1-I7 151.1(8) I8-Cu1-I14[4] 94.2(5) I14[4]-Cu1-I3[3] 72.5(3) I10[3]-Cu2-I25 88.2(10) I15-Cu2-I2[5] 79.8(11) I15-Cu2-I10[3] 109.2(11) I16-Cu2-I2[5] 80.2(11) I16-Cu2-I10[3] 108.0(11) I16-Cu2-I15 136.8(16) I25-Cu3-I10[3] 102.4(6) I15-Cu3-I2[5] 101.8(8) I15-Cu3-I10[3] 104.0(7) I15-Cu3-I16 142.7(9) I16-Cu3-I2[5] 100.6(7) I16-Cu3-I10[3] 99.8(6)	I6-Bi2-I9 90.36(9) I7-Bi2-I9 89.27(9) I8-Bi2-I4 93.17(10) I8-Bi2-I5 89.88(10) I8-Bi2-I6 91.25(10) I8-Bi2-I7 94.27(9) I8-Bi2-I9 176.16(11) I10-Cu1-I10[2] 180.0	I10-Bi2-I13 89.735(18) I11-Bi2-I9 93.35(2) I11-Bi2-I10 93.402(19) I11-Bi2-I12 90.28(2) I11-Bi2-I13 176.86(2) I11-Bi2-I14 90.11(2) I12-Bi2-I10 174.327(19) I12-Bi2-I13 86.593(18) I12-Bi2-I14 97.746(18) I14-Bi2-I10 86.567(17) I14-Bi2-I13 90.00(2) Bi1-I3-Cu1[1] 164.34(4) Cu1-I6-Bi1 166.62(4) Bi2-I9-Cu1 158.28(3) I6-Cu1-I1[2] 165.56(8) I6-Cu1-I9 94.60(6) I7-Cu1-I1[2] 75.01(4) I7-Cu1-I6 101.92(6) I7-Cu1-I8 153.33(8) I7-Cu1-I9 88.18(6) I8-Cu1-I1[2] 78.32(4) I8-Cu1-I6 103.95(6) I8-Cu1-I9 83.42(6) I9-Cu1-I1[2] 71.34(4)
[1]2-X,1-Y,1-Z	[1]-1+X,-1+Y,+Z; [2]-1+X,+Y,+Z; [3]1+X,+Y,+Z; [4]+X,-1+Y,+Z; [5]1+X,1+Y,+Z	[1]-X,1-Y,-Z; [2]1/2-X,+Y,-Z	[1]1-X,1-Y, [2]-Z; 2+X,-1+Y,+Z	

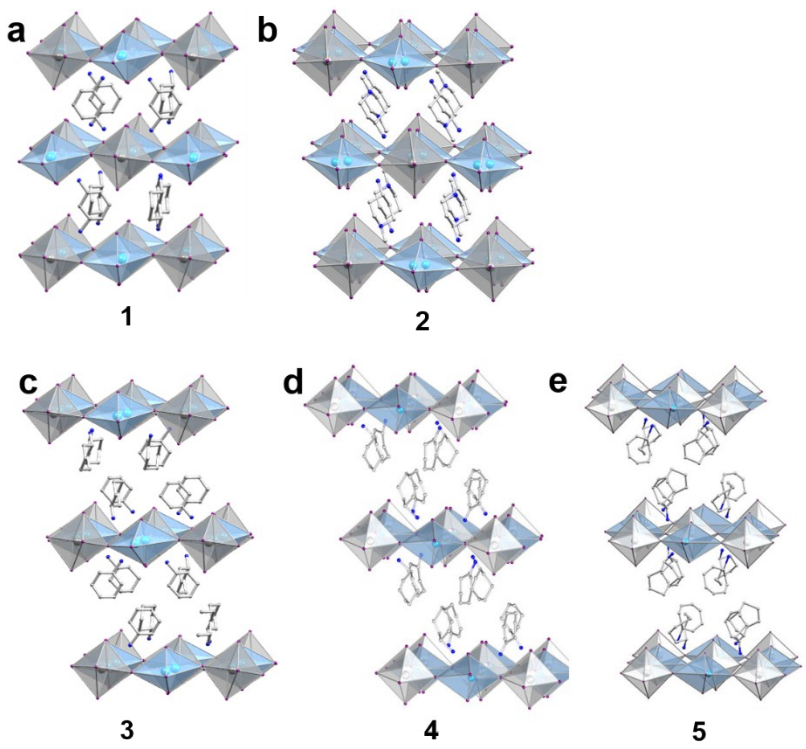

Figure S1 The 3D packing diagram of **1 - 5**

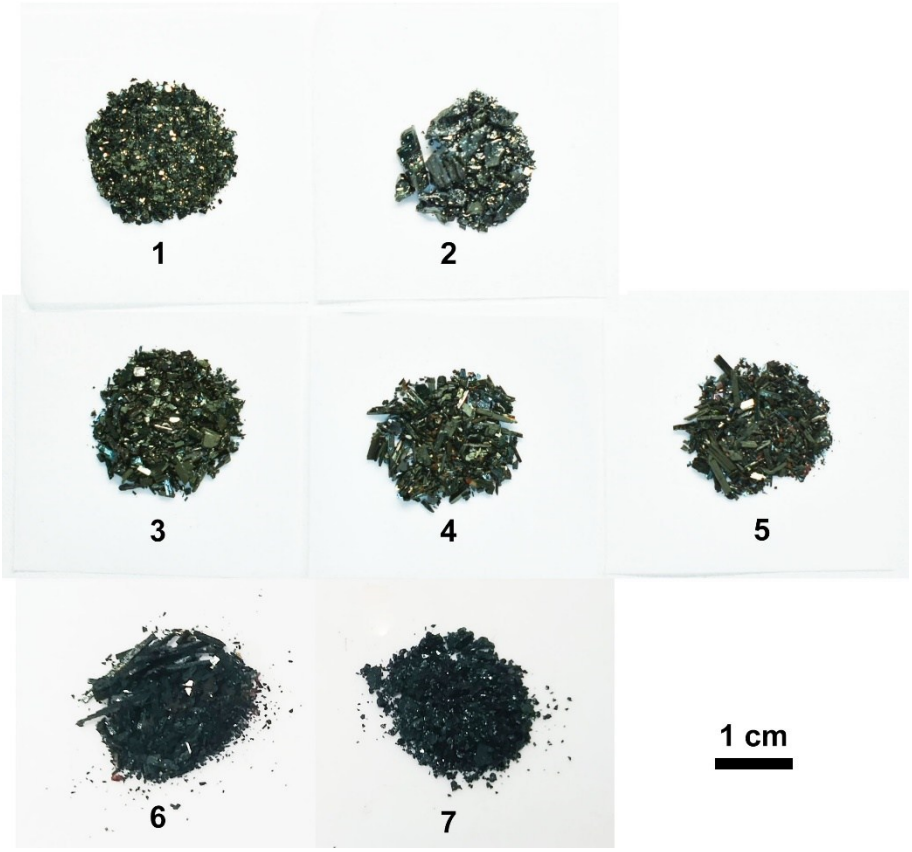

Figure S2 The crystal photographs of **1 - 7**

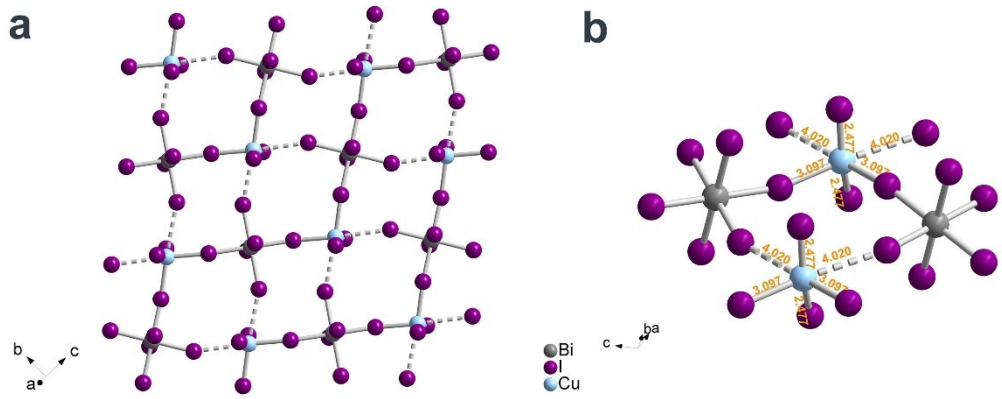

Figure S3. The layered structure of **1**.

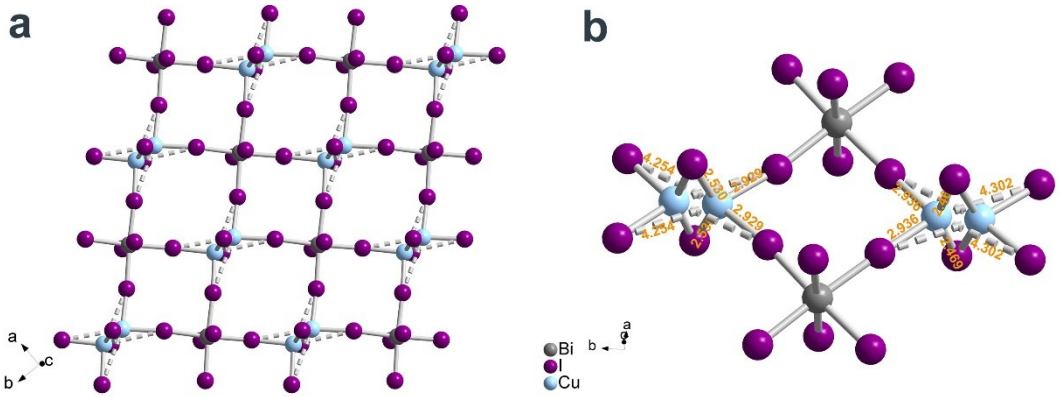

Figure S4. The layered structure of **2**. The occupancy of every Cu is 0.5.

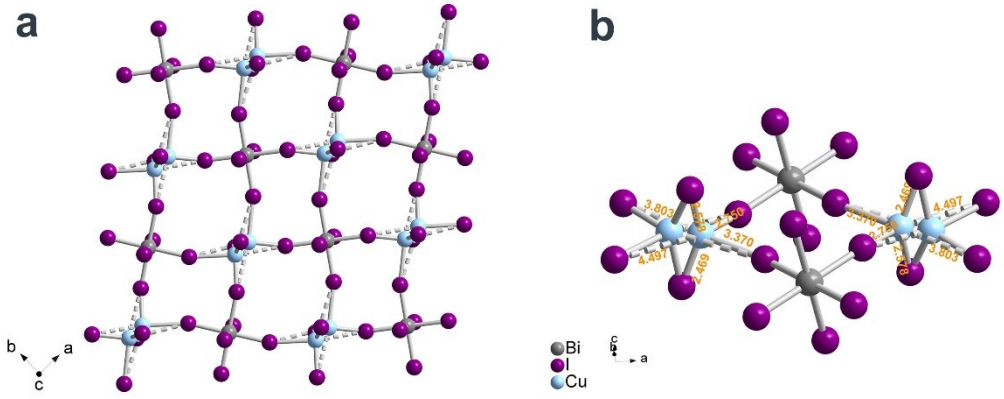

Figure S5. The layered structure of **3**. The occupancy of every Cu is 0.5.

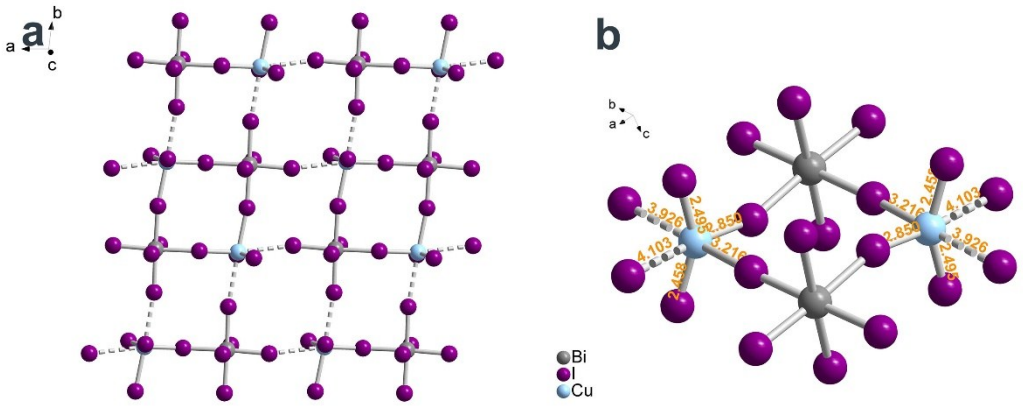

Figure S6. The layered structure of **4**.

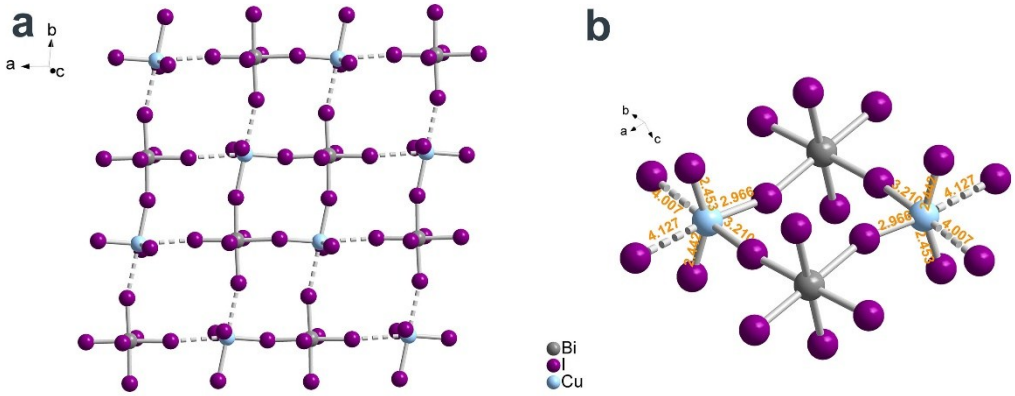

Figure S7. The layered structure of **5**.

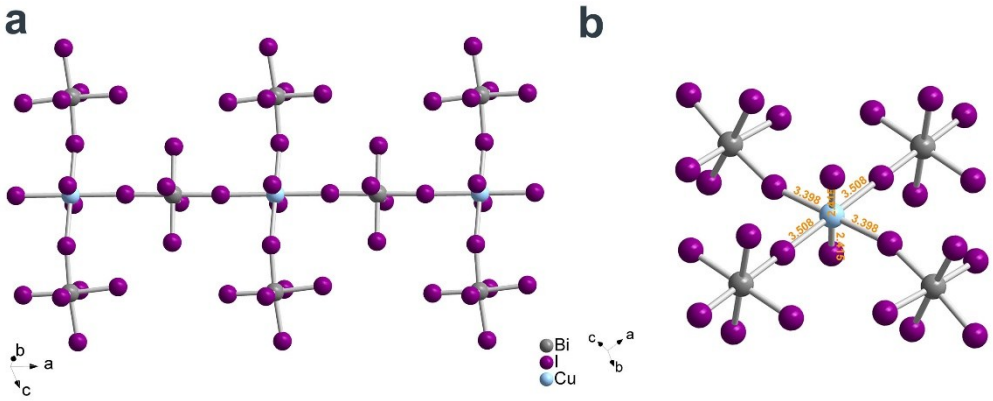

Figure S8. The linear structure of **6**.

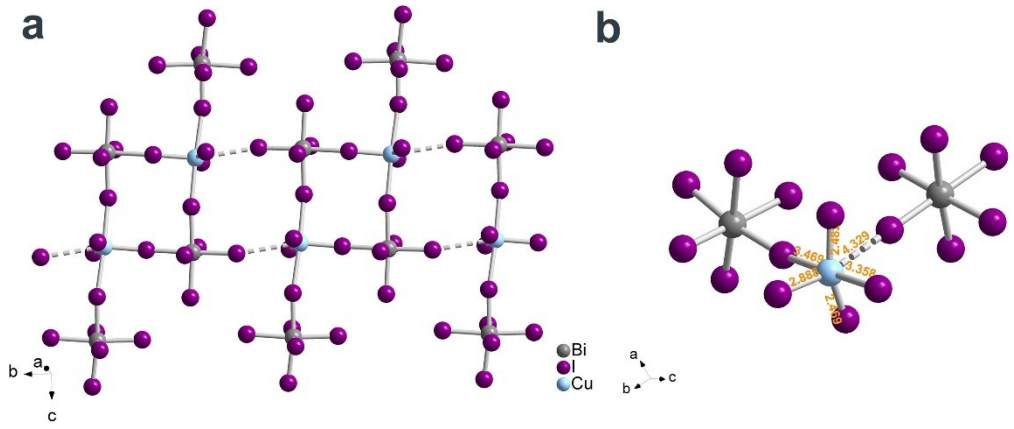

Figure S9. The linear structure of **7**.

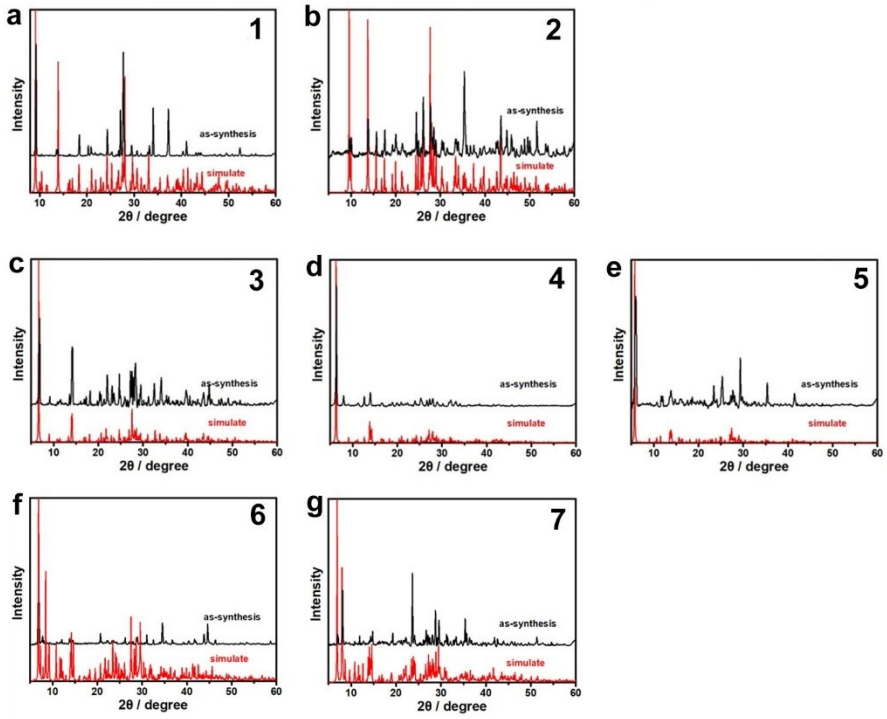

Figure S10 XRD patterns of **1 - 7** powder.

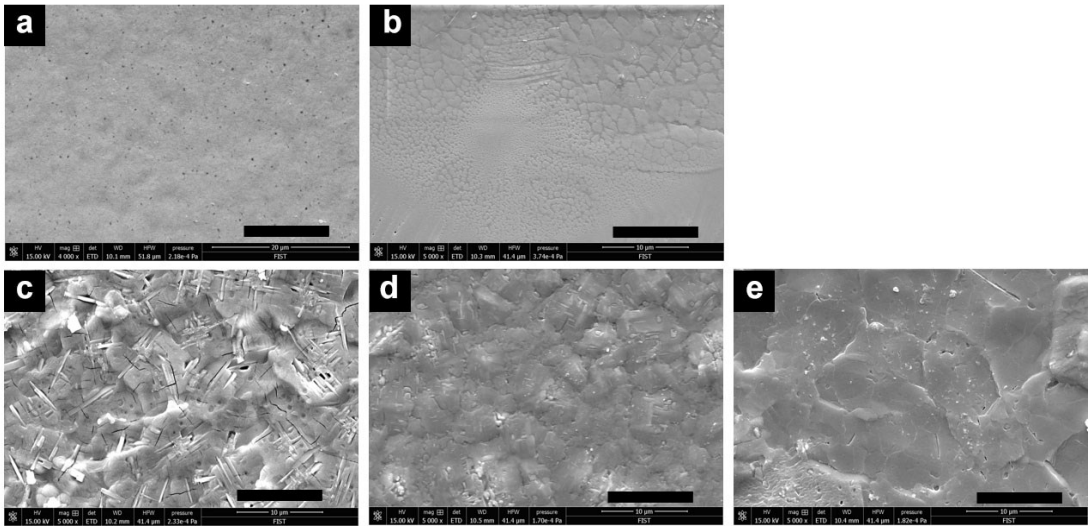

Figure S11 SEM photographs of **1** - **5** films corresponding to a - f respectively. Scale bar 10 μm.

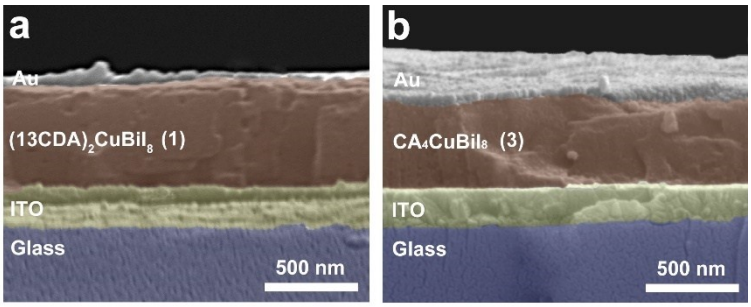

Figure S12 SEM cross section view of **1**, **3** films corresponding to a, b.

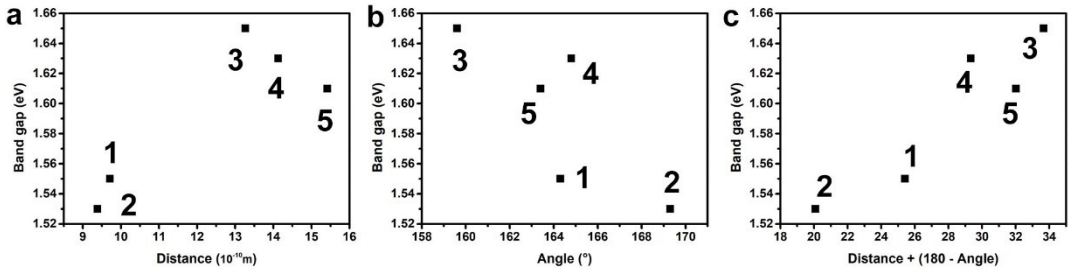

Figure S13 relationship between interlayer distances and band gaps (a); Cu-I-Bi angles and band gaps (b); distance + (180 - angle) and band gaps (c).

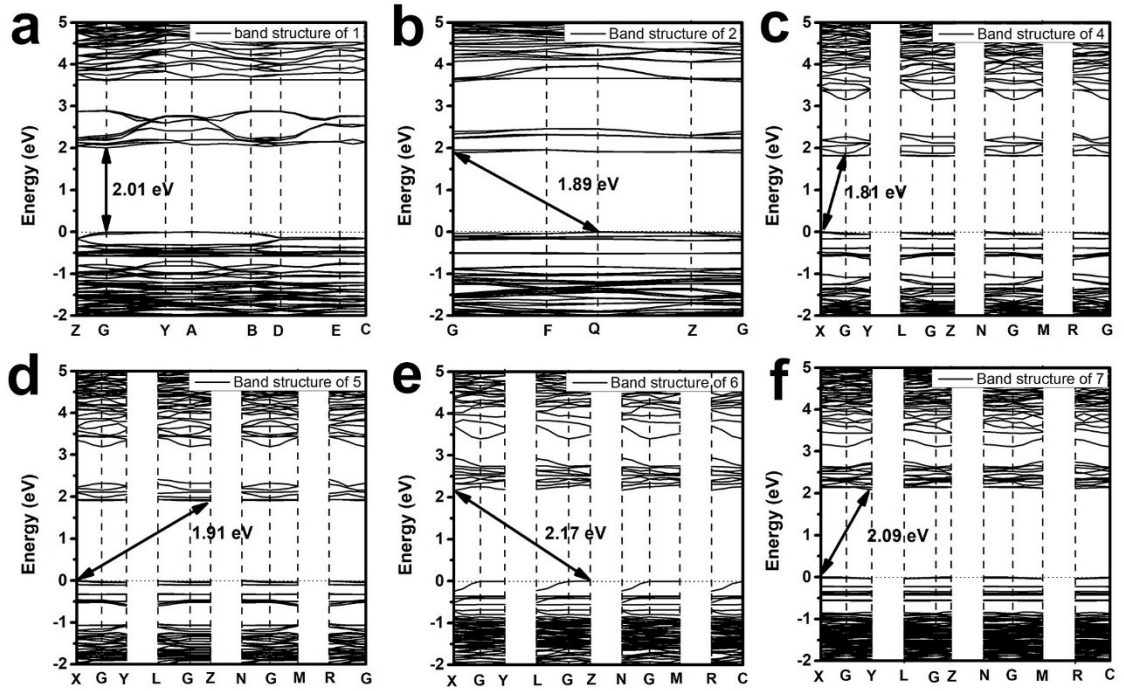

Figure S14 Band structures of compound **1**, **2** and **4** – **7**.

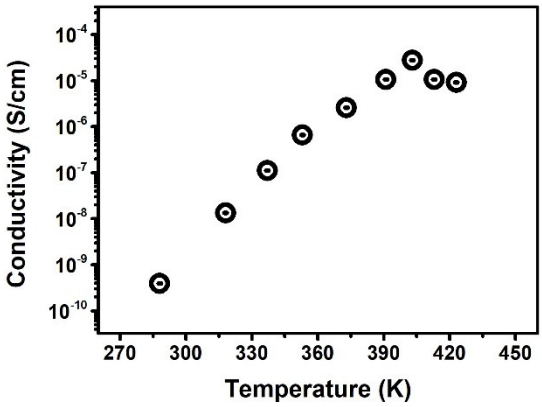

Figure S15 Conductivity as a function of temperature for a pressed pellet of **3**.

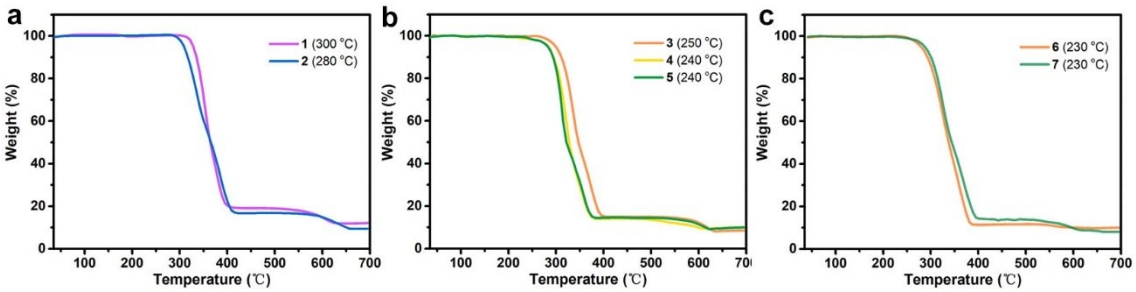

Figure S16 The TGA of **1** – **7**.

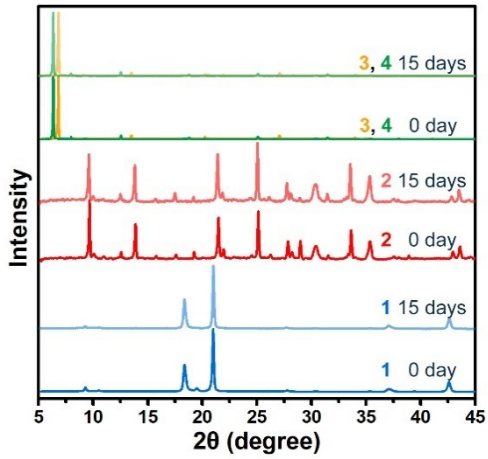

Figure S17 XRD patterns of **1** -**4** films before and after exposure to humidity (90% humidity) for 15 days.

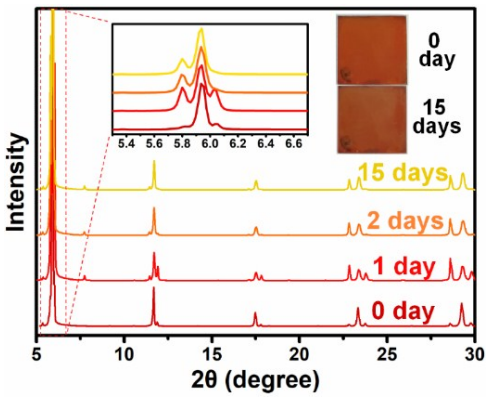

Figure S18 XRD patterns of fresh and aged (1, 2 and 15 days, 90% humidity) films of **5**.